energies

Article

Multi-Objective Optimization of Organic Rankine Cycle (ORC) for Tractor Waste Heat Recovery Based on Particle Swarm Optimization

Wanming Pan [1], Junkang Li [1], Guotao Zhang [1,2], Le Zhou [1] and Ming Tu [1,3,*]

1 College of Engineering, Huazhong Agricultural University, Wuhan 430070, China
2 School of Mechanical Science & Engineering, Huazhong University of Science and Technology, Wuhan 430074, China
3 Key Laboratory of Agricultural Equipment in Mid-lower Reaches of the Yangtze River, Ministry of Agriculture and Rural Affairs, Wuhan 430070, China
* Correspondence: mingtu@mail.hzau.edu.cn

Abstract: Diesel engines are widely used in agricultural tractors. During field operations, the tractors operate at low speed and high load for a long time, the fuel efficiency is only about 15% to 35%, and the exhaust waste heat accounts for 38% to 45% of the energy released from the fuel. The use of tractor exhaust waste heat can effectively reduce fuel consumption and pollutant emissions, of which the organic Rankine cycle (ORC)-based waste heat recovery conversion efficiency is the highest. First, the diesel engine map is achieved through the test rig, a plate-fin evaporator is trial-produced based on the tractor size, and the thermodynamic and economic performance model of the ORC are established. Then, taking the thermal efficiency of ORC and the specific investment cost (SIC) as the objective function, the particle swarm optimization (PSO) algorithm and the technique for order of preference by similarity to ideal solution (TOPSIS) decision method were used to obtain the optimal operating parameter set under all working conditions. Finally, the results showed that the ORC thermal efficiency could reach a maximum of 12.76% and the corresponding SIC value was 8539.66 $/kW; the ORC net output power could be up to 8.31 kW compared with the system without ORC; and the maximum brake specific fuel consumption (BSFC) could be reduced by 8.3%. The improvement in the thermodynamic performance will lead to a sacrifice in economic performance, and at high speeds, the economic benefits and thermal efficiency reach a balance and show a better thermal economic performance. Recovering exhaust heat energy through ORC can reduce tractor fuel consumption and pollution emissions, which is one of the effective technical means to achieve "carbon neutrality" in agricultural production. At the same time, through the PSO algorithm, the optimal combination of ORC operating parameters is obtained, which ensures that the exhaust heat energy can be effectively recovered during the tractor field operation, and provides a basis for the adjustment of real-time work strategies for future research.

Keywords: multi-objective optimization; organic Rankine cycle; tractor diesel engine; PSO; TOPSIS

Citation: Pan, W.; Li, J.; Zhang, G.; Zhou, L.; Tu, M. Multi-Objective Optimization of Organic Rankine Cycle (ORC) for Tractor Waste Heat Recovery Based on Particle Swarm Optimization. *Energies* **2022**, *15*, 6720. https://doi.org/10.3390/en15186720

Academic Editor: Constantine D. Rakopoulos

Received: 31 July 2022
Accepted: 12 September 2022
Published: 14 September 2022

1. Introduction

Since the 21st century, the demand for tractors has increased with the continuous development of agriculture in China. As a significant part of agricultural production and having the characteristics of high production efficiency and low unit cost, the number of tractors has increased from 15.80 million in 2004 to 23.17 million in 2020, and the total power of the country's agricultural machinery reached 1.056 billion kilowatts [1]. China's tractor market is a typical stock market, and the increase in tractor ownership and total agricultural machinery power indicates that China's agricultural production has shifted from relying mainly on human and animal power to mechanical power, entering a new period of mechanization. China is continuing to promote the full mechanization of agricultural production, which shows that agricultural modernization is in a critical period of changing the development mode, and the use and ownership of tractors will continue to increase in the coming period.

As agricultural machinery with the longest average annual working time (more than 500 h) [2], tractors are increasingly used in agricultural production, and the problem of their energy consumption and pollutant emissions is gradually attracting attention [3,4]. The diesel engine is widely applied in tractors and has accounted for more than 95% of the agricultural machinery power source; tractors operate at a constant speed most of the time with long working hours and heavy load, so a large amount of exhaust waste heat energy is lost directly to the air, failed to be effectively used, and has been recognized as a notable source of pollutant emissions, contributing to poor air quality and negative impacts on human health [5].

What calls for special attention is how to reuse the exhaust waste heat energy to improve the fuel efficiency and reduce emissions. In recent years, with the increasing environmental pollution and energy dependence, the traditional diesel engine energy saving, and emissions reduction have been of wide concern, but in the field of agricultural machinery, tractor diesel engine waste heat recovery (WHR) and energy reuse have not yet attracted sufficient attention. Diesel engine fuel efficiency during tractor operation in the field is only 15% to 35%, and exhaust energy accounts for 38% to 45% of the energy released from the fuel, so recycling the reuse of exhaust waste heat can help improve fuel utilization and reduce emissions. Research has shown that the WHR based on the organic Rankine cycle (ORC) has the highest exhaust heat energy conversion rate [6]. Punov et al. [7] presented the possibilities of exhaust heat recovery for a 110 kW tractor engine and the simulations results revealed that the engine output power and efficiency increased within the range of 3.9–7.5%. At full load, the calculated exhaust enthalpy was within the range of 32.1 kW to 103.4 kW, as the corresponding temperature varied from 693 K to 785 K. At full engine load, 8.36–14.8% of the fuel energy can be converted into mechanical work. ORC is considered as a promising heat-to-power technology to utilize waste heat and renewable energy. However, since the thermodynamic, economic, and environmental performance is usually in conflict, a single objective design can no longer meet the ORC system requirements, and the urgent requirements for multi-objective optimization have attracted increasing attention [8]. As the most widely used means of transportation today, automobiles have caused a lack of energy due to the rapid increase in their numbers. How to improve energy utilization to achieve energy saving and emissions reduction has attracted a series of scholarly research on automobiles. ORC technology has received extensive attention due to its superior performance. Although the current research on ORC for diesel engine WHR is now concentrated in the field of on-road vehicle engineering, the WHR of tractors, which also use diesel engines as a power source, can utilize similar research methods and technical means.

In the cases of off-highway vehicles, it is possible to observe stable high speed and torque profiles during operations for agricultural tractors. Lion et al. [9] assessed the possibility of applying an ORC system in a commercial agricultural tractor, recovering waste heat from a 300 kW power heavy-duty diesel engine. A maximum fuel consumption reduction of 10.6% was obtained using heat from the tailpipe and EGR. Different WHR technologies including ORC to be used in agricultural applications were analyzed [10]. More than 80% of the time, the engine operated at high load and almost constant speed when the tractors are run on the fields; at full engine load, the exhaust heat is lost to the environment in the form of power from 42.5 kW to 139.9 kW with the temperature varying from 700 K to 800 K. The exergetic analysis showed that a maximum of 15% of fuel low heating value can be reused by employing ORC, and at the most typical operation points, this value is from 10% to 12.8% [11].

The existing research is mainly on tractor steady-state operating conditions or for a single, stable heat source condition; there has been less analysis of tractors in off-design performance or variable operating conditions of the ORC operating state as well as the impact on system stability, where system optimization has not been achieved. Therefore, the focus and difficulty of the research have changed from the energy conversion efficiency of the ORC at a single, stable design operating point to how to dynamically adjust the ORC operating parameters and the synergistic matching with the exhaust heat energy to ensure the operational stability and effectiveness of the system under variable operating conditions [12,13]. A good design of an ORC system for tractor applications should be lightweight, a small size, low cost, evaporator pressure drop, high net power output, better off-design performance, and high controllability [14]. The most appropriate way to solve these problems is to perform multi-objective optimization. At present, the solutions in relevant research are roughly divided into two types. One is to predict through simulation, and the other is to optimize through intelligent algorithms combined with neural networks. In addition, due to the actual operation process, the collection of data such as flow, temperature, speed, and other data at each operating point consumes a lot of manpower, financial resources, and energy. Therefore, in the research, it is often necessary to process the data and conduct correlations based on the existing data. In recent years, due to the advantages of self-adaptation, self-learning, nonlinear mapping, and fault tolerance, neural networks with optimization algorithms such as particle swarm optimization (PSO) have proven to be an effective tool for design and performance optimization in the field of thermal engineering.

System optimization based on the PSO algorithm was performed to indicate the development potential of the ORC system, and the PSO was employed to optimize the parameters of pulsating flow when a diesel engine operates under the motorway road condition [15,16]. The multi-objective genetic algorithm (MOGA) was used to optimize three combined heat and power based on ORC systems, respectively, to achieve higher exergy efficiency and profit ratio of investment [17]. Additionally, the PSO was used to optimize the net output power as the objective function, and results revealed that the overall thermal and exergy efficiencies were obtained at 18.23% and 62.37%, respectively, for the base case [18]. A reliable and time-efficient optimization tool was developed in the MATLAB environment that was able to optimize ORC, the genetic algorithm (GA) toolbox was used, and the fluids' thermophysical properties were acquired from the CoolProp [19] and REFPROP [20] databases [21]. A machine learning prediction model was developed and applied to predict the ORC power output, GA was used to optimize the initial weights and thresholds of the different structural parameter ORC model to further improve the model generalization ability [22]. A simulation model of an ORC fin-and-tube evaporator via the computational fluid dynamic method was established, where the evaporator with a nonuniform structure obtained by GA optimization could further enhance the heat transfer and improve the flow state of the evaporator [23]. Based on machine learning, the GA and PSO were combined into a GA–PSO hybrid algorithm to predict and optimize the pump isentropic efficiency under full operating conditions in an ORC system [24]. The performances of GA, PSO, and repulsive particle swarm optimization (RPSO) based on the optimization of thermo-economic indicators were compared as well as in the optimization of the thermodynamic process of an ORC energy recovery system [25]. A multi-objective optimization using the PSO algorithm aimed at the proposed heat exchanger was conducted and the optimal design scheme had the potential to achieve a 71.46% decrease in the total annual cost [26]. A novel thermo-economic performance indicator, namely, maximum net power output with the constraint (MPC), was proposed, and the organic and steam Rankine cycle systems driven by the flue gas were optimized to maximize the net power output with the constraint of electricity production cost by using the non-dominated sorting genetic algorithm-II [27]. Performance prediction and multi-objective optimization using a back propagation neural network (BPNN) were investigated, an ORC experiment platform was used to obtain 950 sets of basic experimental data, the results demonstrated that the prediction error of the BP-ORC model was very low, and the system performance could be improved by adjusting several operating parameters experimentally according to the model prediction [28]. A comprehensive method to achieve a reasonable application of machine learning into ORC research for the prediction and optimization of the ORC's parameters and performance was presented. BPNN and support vector regression (SVR) prediction models for ORC were built by predicting error analysis with part of the database [29]. A preliminary design method was developed to optimize the eight critical parameters of the ORC based on the PSO algorithm; the isotropic efficiency was the objective function and the results indicated that the turbine efficiencies increased with the reduction in the pressure ratio and turbine inlet temperature and the increase in the power output. The exergy efficiency and isotropic efficiency dropped slightly with the increase in the turbine inlet temperature. Therefore, the turbine with R245fa exhibited good off-design performance [30]. PSO with parallel computation was adopted to optimize the performance of the nonlinear ORC system, where the result showed that the optimal system could output 6.87% more power than the initial system and 20.08% more power [31]. A fuzzy nonlinear dynamic model of the ORC evaporator using renowned finite volume (FV) was developed to capture the transient effects accurately, and the results showed that the fuzzy-based model was able to capture the transient effects at a data fitness of over 90% [32]. A control-oriented neuro-fuzzy model of brazed-plate evaporators for use in ORC was built to assess the dynamic performance of the ORC system. The proposed adaptive neuro-fuzzy inference system (ANFIS) model consisted of two separate neuro-fuzzy sub-models to predict the evaporator output temperature and evaporating pressure. The effect of training the models using gradient-descent least-square estimate (GD-LSE) and PSO techniques was investigated [33]. A PSO algorithm was used to optimize the operating parameters of the regenerative ORC system under various engine operating conditions [34]. A multi-objective optimization approach on the PSO for parametric optimization was applied to find a set of Pareto optimal solutions [35]. A multi-condition performance prediction method with the PSO algorithm for ORC centrifugal pumps was proposed and compared with the experimental results, where the performance under multiple operating conditions was well-predicted by introducing performance constraints [36]. To reduce the computation time, a new fuzzy-based evaporator model was developed and the performance compared with the finite volume method. The results showed that the fuzzy technique can be applied to predict the output of the supercritical evaporator in the WHR system and can significantly reduce the required computation time [37]. Considering the great potential of deep reinforcement learning (DRL) for solving complex control problems, a DRL-based energy management system (EMS) was proposed for an HEV-ORC. The simulation results demonstrated that the DRL-based EMS could save 2% more fuel energy than the rule-based EMS [38]. A nonlinear model predictive controller (NMPC) was designed to provide optimal control input for maximum turbine power generation in an ORC–WHR system. The power optimization-based NMPC utilized an extended Kalman filter (EKF) as a state estimator. The working fluid evaporation pressure was controlled by an external PID control loop. The experimental study showed that the augmented control scheme outperformed the baseline multi-loop PID control in terms of both the tracking error and settling time during transient engine operation [39,40]. Most of the existing research in the literature on machine learning has been to collect single indicators such as the ORC thermal efficiency with different ORC operating parameters including the working fluid mass flow rate, pressure, etc. at a single engine operating condition, then build a neural network to predict and find the optimal value in a given range of ORC operating parameters, which means the amount of data needed to be collected and trained for each of the engine operating conditions. However, this research method often only considers a single indicator and not all of the engine operating conditions are available in all cases.

The current research literature on exhaust waste heat recovery based on ORC has mainly focused on the technical economy and thermodynamic performance of the systems under engine on-design operating conditions by means of experimental data and simulations. However, in the operation of the tractor, there are differences in the engine speed and load under the switching of different working modes such as field tillage, headland steering, and idle parking, which lead to system instability due to low degree superheating of the working fluid at the evaporator outlet. Therefore, the study of the tractor exhaust heat transfer law with the ORC combined and how to determine the operating range and predictive the performance of the ORC parameters under off-design conditions was the research question of this paper. In order to ensure the efficient and stable operation of the system, the parameters of the working fluid and coolant water such as the pressure, degree of superheat and subcooling, and mass flow rate were selected as the optimization parameters, and the thermal efficiency of ORC and the economic performance indicators were used as the objective functions. Compared to the several implementations presented with machine learning, the PSO algorithm combined the technique for order of preference by similarity to ideal solution (TOPSIS) decision-making were adopted to solve the Pareto frontier and optimize the parameter combinations, respectively. The optimal parameter combinations and distributions were determined under all operating conditions and the validity of the model was verified by comparing the experimental data with the PSO optimization model and the prediction results of the BPNN. The rest of this paper is organized as follows. In Section 2, the universal characteristic data of the diesel engine are obtained through the test rig, the detailed thermodynamic and economic performance model of each component of the ORC are established, and a multi-objective optimization model is built on this basis. In Section 3, single and multi-operating conditions optimization and thermo-economic optimization are analyzed. The conclusions are presented in Section 4.

2. Materials and Methods

2.1. System Description

The aim of this research was to study the exhaust heat potential of the engine under all operating conditions, and how the thermodynamic parameters of the ORC working fluid are adapted to the engine operating conditions and exhaust parameters to ensure that the exhaust heat energy can be effectively utilized. Therefore, it is necessary to measure the brake power, brake specific fuel consumption (BSFC), exhaust temperature, pressure, and mass flow rate of the engine under all operating conditions. In this paper, an eddy current dynamometer was used to measure the 4-cylinder, 4-stroke, 1.9 L turbocharged diesel engine brake power, torque, and speed; a NI 4-slot, Ethernet chassis cDAQ-9184 combined with four modules was employed to build a test data acquisition system. The exhaust data of the diesel engine at 210 operating points were collected. Figure 1 shows the brake power and exhaust temperature of the diesel engine under all operating conditions, the maximum torque and rated power were 361.4 N-m at 2250 rpm and 118.7 kW at 3500 rpm, respectively, the exhaust temperature increased with the engine speed and load, and the highest exhaust temperature was 950 K with the engine speed of 4000 rpm at full load.

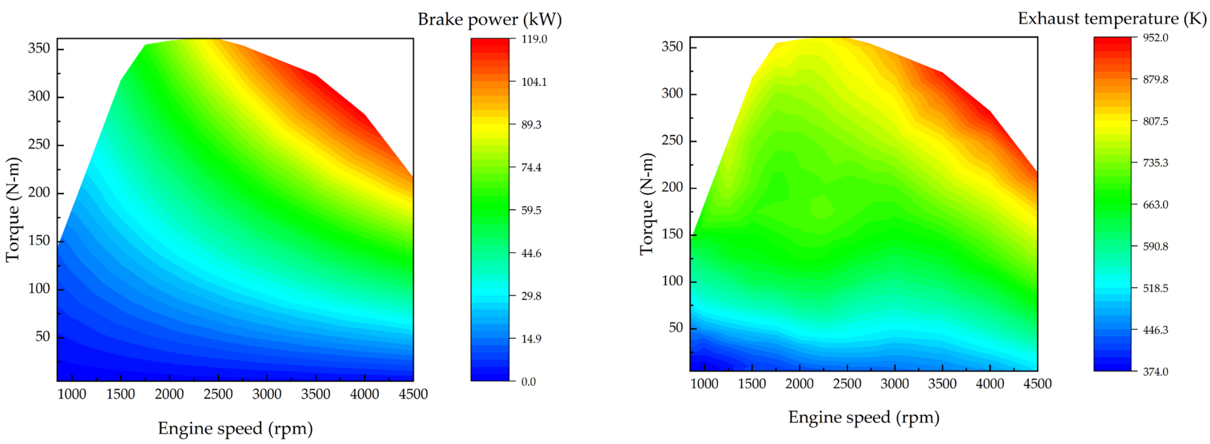

(**a**) (**b**)

Figure 1. Diesel engine MAP: (**a**) engine brake power; (**b**) engine exhaust temperature.

According to the variation law of the exhaust energy of a vehicle diesel engine, a set of the ORC system was designed, the diesel engine was used as the top cycle, the working cycle of the ORC system was used as the bottom cycle, and the combined system of the engine–ORC was constructed. The conceptual schematic of the engine–ORC system is shown in Figure 2, where R245fa was selected as the organic working fluid for circulation. As a key component of the ORC, the analysis of the thermal performance of the evaporator under the space constrained condition of the tractor can provide a theoretical basis for the optimal design of the evaporator parameters as well as effectively improve the utilization of the exhaust heat of the tractor. Therefore, in this paper, after the actual measurements of the front space of the hood and the dimensions of the cab roof of three different horsepower tractors such as Dongfanghong 804/854/954, a plate fin evaporator was made on a trial basis. The experimental evaporator was constructed from aluminum heat-sink stock, which consists of three separate heat exchangers; the evaporator structural sketch and dimensional parameters are shown in Figure 3 and Table 1. It consisted of three separate heat exchangers, the thicker middle section as the hot-side for the engine exhaust and the two outer sections as the cold-side designed for the ORC working fluid flow. The thicker middle section was constructed using two identical sections of heat-sink material, the fins of one side, while facing the fins of other, were inserted into the gaps between the fins of the opposing side, resulting in a fin spacing one-half that of the heat sink material. The fin height is therefore equal to the fin height of the original heat sink stock.

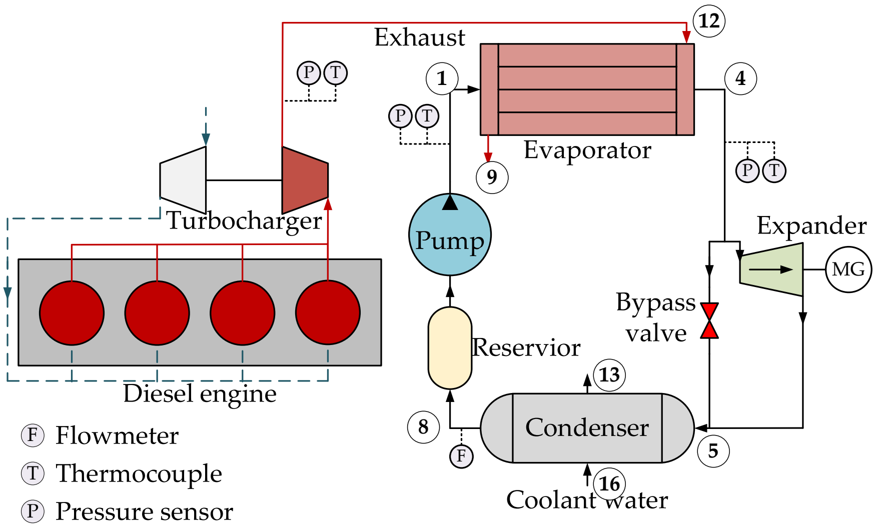

Figure 2. The conceptual schematic of the engine–ORC system.

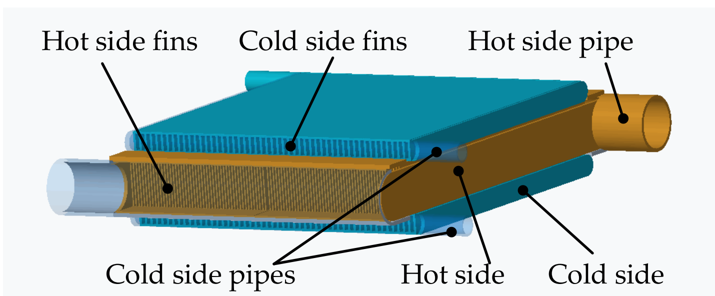

Figure 3. A 3D evaporator assembly drawing.

Table 1. The experimental plate fin evaporator parameters.

Parameter	Hot Side	Cold Side
Pipe diameter/cm	8.00	2.50
Flow channel/cm	50.00	50.00
Fin height/cm	6.35	2.55
Fin thickness/cm	0.30	0.25
Fin space/cm	0.35	1.00
Number of flow channel	102	96

2.2. ORC Model Description

Figure 4 shows the working fluid R245fa T-S diagram. State points from 1 to 8 indicate the working fluid cycle, state points 9 to 12 indicate the engine exhaust cooling process, and state points 13 to 16 indicate the coolant water heating process. According to the figure, the thermodynamic model of the engine–ORC system was established.

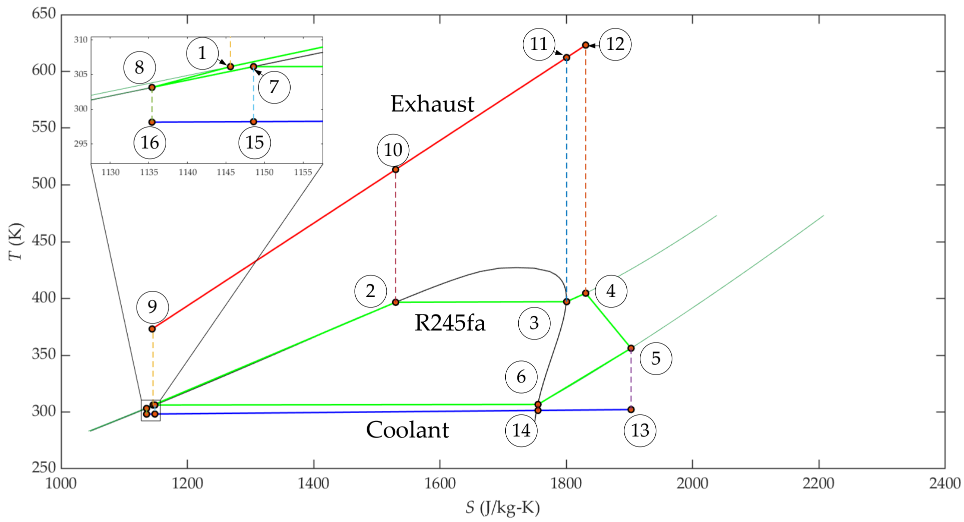

Figure 4. The T-S diagram with the state points.

Process 1–4: The working fluid starts a cycle as the liquid leaving the pump at state point 1, then is preheated to saturation and evaporated through the evaporator. The heat absorbed from the exhaust gases is calculated in Equation (1), the specific enthalpy *i*, and the temperature of each state point can be calculated from the energy balance equation.

$$\dot{Q}_{in} = \dot{m}_r(i_4 - i_1) = \dot{m}_e(i_{12} - i_9) \tag{1}$$

where $\dot{m}_r$ and $\dot{m}_e$ are the mass flow rate of R245fa and the exhaust gases, respectively.

The evaporator, as a counter-flow finned heat exchanger, was modeled using log mean temperature difference (LMTD), considering the three-zone method, as shown in Figure 5. The thermodynamic evaporator model was developed for this paper to establish the thermodynamic model of the evaporator, and the following assumptions were made to simplify the numerical calculation procedure.

(1) Ignore the heat dissipated by the evaporator to the environment;
(2) Ignore evaporator fouling factor and material thermal resistance;
(3) Ignore the changes in heat conduction, potential energy and kinetic energy of the evaporator fluid along the axis of the flow channel and pipeline.

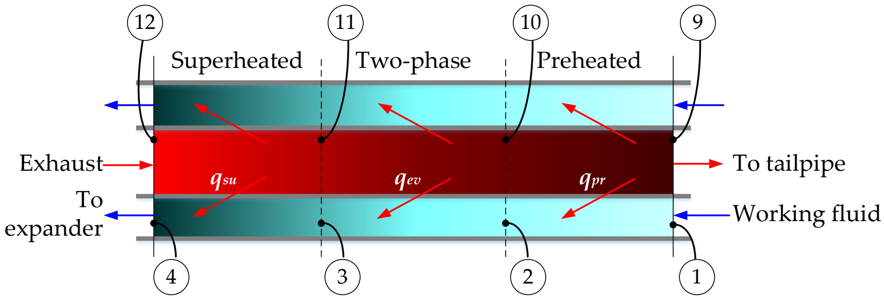

Figure 5. A schematic diagram of the evaporator dynamic model.

The thermodynamic properties of the R245fa refrigerant and diesel exhaust gases such as the specific heat and the convection heat transfer coefficient were sourced from an online property calculator developed and maintained by the National Institute of Standards and Technology (NIST) [20]. Thermodynamic properties of the diesel engine exhaust gases were derived from known air and flue mass flow rates and assuming the complete combustion of the fuel having assumed the molecular structure of dodecane ($C_{12}H_{26}$).

The cross-sectional area of the evaporator pipe was circular, while the cross-sectional area of the flow channel was rectangular. Considering the convective heat transfer in the tube with different cross-sectional shapes, the Nusselt number Nu of R245fa and exhaust gas was calculated by Equation (2) [41]. The respective heat transfer coefficients h_r and h_e of R245fa and exhaust gas, the total heat transfer coefficient U of the evaporator, and the heat transfer area A can be calculated from the structural parameters and the LMTD method, as shown in Equations (3)–(5), where the two-phase heat transfer coefficient h_{ev} is determined by Equation (6).

$$Nu = \frac{a_0}{4.36} \cdot 0.023 Re^{4/5} Pr^{0.3} \tag{2}$$

$$h = k \cdot Nu/D \tag{3}$$

$$U = \frac{1}{1/h_r + 1/h_e} \tag{4}$$

$$A = \frac{q}{U \cdot \Delta T} \tag{5}$$

$$h_{ev} = \left[(Fh)^2 + \left(Sh_{pool} \right)^2 \right]^{1/2} \tag{6}$$

where a_0 is the scaling factor, 8.24 for the exhaust gases, and 5.39 for the working fluid, respectively. Re is the Reynolds number based on hydraulic diameter, Pr is the Prandtl number, k is the thermal conductivity of the fluid, D is the hydraulic diameter of the flow channel calculated by the parameters in Table 1, F and S are the forced convective heat transfer enhancement factor and suppression factor, respectively, h_{pool} is the pooling boiling transfer coefficient [42].

Process 4–5: Saturated vapor from the evaporator at state 4, having an elevated temperature and pressure, expands through the expander to produce work and is then discharged to the condenser at state 5 with relatively low pressure. Neglecting heat transfer with the surroundings, the mass and energy rate balances for a control volume around the expander reduce at the steady state to give:

$$\dot{W}_{exp} = \dot{m}_r (i_4 - i_5) = \dot{m}_r (i_4 - i_{5s}) \cdot \eta_{exp,iso} \tag{7}$$

where $\eta_{exp,iso}$ is the isentropic efficiency of the expander.

Process 5–8: In the condenser, there is heat transfer from the working fluid to the cooling water. The working fluid condenses and the temperature of the cooling water increases; heat emitted from the work fluid to the cooling water is expressed in Equation (8). The modeling approach for the thermodynamic model of the condenser is similar to that of the evaporator, while the overall structure is half the size of the evaporator.

$$\dot{Q}_{out} = \dot{m}_r(i_5 - i_8) = \dot{m}_c(i_{13} - i_{16}) \tag{8}$$

Process 8–1: The working fluid condensate leaving the condenser at 8 is pumped from the condenser into the higher-pressure evaporator. Taking a control volume around the pump and assuming no heat transfer with the surroundings, the mass and energy rate balances give

$$\dot{W}_{pump} = \dot{m}_r(h_{1s} - h_8) = \dot{m}_r(h_1 - h_8) \cdot \eta_{pump,iso} \tag{9}$$

where $\eta_{pump,iso}$ is the isentropic efficiency of the pump.

The thermal efficiency gauges the extent to which the energy input to the working fluid passing through the evaporator is converted to the net output power. Using the quantities and expressions introduced above, the thermal efficiency η_{ORC} of the ORC system is

$$\eta_{ORC} = \frac{\dot{W}_{exp} - \dot{W}_{pump}}{\dot{Q}_{in}} \tag{10}$$

2.3. Economic Model

The thermodynamic model of the ORC described in the previous section was expanded by considering the costs of the main elements in the cycle. These costs were estimated from the work of Lecompte et al. [43] and Quoilin et al. [44], and are presented in Equation (11). The total cost (TC) of the ORC system is mainly dependent on the component costs, C_{cp}, and labor cost, C_{lab}, which is half of the C_{cp}. The cost calculation of common components should include the ORC heat exchanger, expander, pump, electric motor, and working fluid, and refer to the NETL (National Energy Technology Laboratory) and the results provided by Pantaleo [45]

$$TC = C_{cp} + C_{lab} \tag{11}$$

The cost correlation is based on the heat exchanger heat transfer area A:

$$C_{b,hx} = \exp\{7.15 + 0.16[\ln(10.8A)]\} \tag{12}$$

The heat exchanger cost, C_{hx}, is determined from:

$$C_{hx} = F_P F_M C_{b,hx} \tag{13}$$

where

$$F_P = 0.851 + 0.129\left(\frac{p - 101300}{41.4}\right) + 0.0198\left(\frac{p - 101300}{41.4}\right)^2 \tag{14}$$

where F_p is the pressure factor and F_m is the material factor, F_m is set to 2.

As screw compressors can be modified to operate in reverse mode as expanders, the correlation from Astolfi [46] was used, where the size parameter is the volumetric flow rate at the outlet of the expansion, and the expander cost C_{exp} is expressed in Equation (15). The pump cost expression C_{pump} is shown in Equation (16)

$$C_{exp} = 3144 + 217400\dot{V}_{out} \tag{15}$$

$$C_{pump} = 900 \cdot \left(\frac{\dot{W}_p}{300}\right)^{0.25} \tag{16}$$

The cost of the electric motor that drives the pump is C_{motor}:

$$C_{motor} = \exp\left\{ \begin{array}{c} 5.83 + 0.131\left[\ln\left(1.341\dot{W}_p\right)\right] + 0.0533\left[\ln\left(1.341\dot{W}_p\right)\right]^2 \\ +0.0286\left[\ln\left(1.341\dot{W}_p\right)\right]^3 - 0.00355\left[\ln\left(1.341\dot{W}_p\right)\right]^4 \end{array} \right\} \tag{17}$$

The working fluid cost C_{wf} is determined by the mass:

$$C_{wf} = 20 \cdot m \tag{18}$$

Therefore, the estimate TC is equal to the result of the component costs and the labor costs, and the specific investment cost (SIC) is used as the thermo-economic objective function.

$$TC = 1.5 \cdot \left(C_{hx} + C_{exp} + C_{pump} + C_{motor} + C_{wf}\right) \tag{19}$$

$$SIC = \frac{TC}{\dot{W}_{exp} - \dot{W}_{pump}} \tag{20}$$

2.4. Multi-Objective Optimization Model

Based on the above analysis, the size of the diesel exhaust heat is mainly determined by the operating conditions, and the distribution characteristics of the exhaust energy will change with the engine operating conditions. Since the ORC system involves multiple operating parameters and the coupling between each parameter, it is difficult to analyze the performance of the ORC under variable engine operating conditions and the relationship between the operating parameters simply through the sensitivity analysis. Therefore, in this paper, a multi-objective optimization model was established to optimize the main operating parameters of the ORC system, and the solution was solved by the PSO algorithm. Figure 6 shows the flow chart of the PSO algorithm established in this paper.

The particle swarm algorithm simulates a bird in a flock by designing a massless particle with only two properties: velocity and position, where velocity represents the speed of movement and position represents the direction of movement. Each particle searches for the optimal solution independently in the search space, which is recorded as the current individual extreme value, and shares the individual extreme value with other particles in the entire particle swarm. All particles in the particle swarm find the current individual extreme value according to their own. The current global optimal solution shared with the entire particle swarm adjusts its speed and position.

In this paper, the ORC thermal efficiency η_{ORC} and SIC were used as the objective function, and the evaporation pressure, condensation pressure, mass flow rate, degree of superheating and subcooling of the working fluid, and the mass flow rate of the coolant water were selected as the decision variables. The multi-objective optimization mode can be expressed as:

$$max(\eta_{ORC}) = f_1(P_1, P_5, \Delta T_{34}, \Delta T_{78}, \dot{m}_r, \dot{m}_c) \tag{21}$$

$$max(SIC) = f_2(P_1, P_5, \Delta T_{34}, \Delta T_{78}, \dot{m}_r, \dot{m}_c) \tag{22}$$

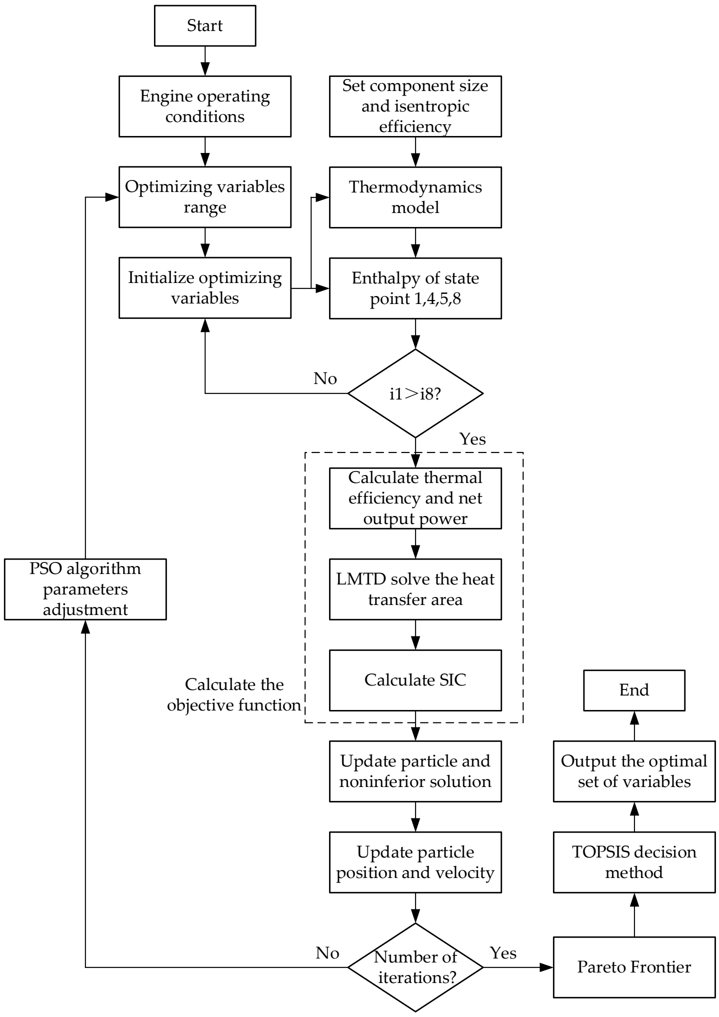

Figure 6. Flow chart of the PSO algorithm.

The value ranges of the optimization variables were set as shown in Table 2.

Table 2. The value ranges of the optimization variables *.

Variables	Lower Limit	Upper Limit
P_1/MPa	1	3
P_5/MPa	0.1	0.5
ΔT_{34}/K	1	20
ΔT_{78}/K	0	10
$\dot{m}_r$/kg·s^{-1}	1 to 1.5 times the corresponding exhaust mass flow rate.	
$\dot{m}_c$/kg·s^{-1}	0.08	0.15

* P_1 and P_5 represent the pressure of the working fluid at the inlet of the evaporator and condenser, respectively; ΔT_{34} and ΔT_{78} represent the degree of superheating and subcooling of the working fluid in the evaporator and condenser, respectively; $\dot{m}_r$ and $\dot{m}_c$ represent the mass flow rate of working fluid and the mass flow rate of coolant water, respectively.

Since the objectives in multi-objective optimization are often mutually constrained, optimizing one of the objectives must be performed at the expense of degrading the performance of the other objectives. The difference with single-objective optimization is that instead of a unique optimal solution, there is an optimal solution set, which is explained by a concept in economics—the Pareto solution set. The frontier formed by the Pareto solution is also called the Pareto frontier. For practical problems, it is often necessary to pick one or more solutions from the Pareto solution set as the optimal solution to the problem to be solved. The setting of the algorithm parameters of the optimization model has a great influence on the optimization results. When applying the particle swarm algorithm for solving multi-objective optimization problems, the optimized model needs to be calibrated. The algorithm parameters involved mainly include the population size, number of iterations, mutation probability, learning factor, etc. Taking the rated working condition of the diesel engine as an example, to verify the optimization model, the optimal parameter setting should make the Pareto front obtained by the multi-objective optimization evenly distributed in a small area.

Figure 7 shows the Pareto frontier results of different population numbers. The population numbers were set as 10, 20, 30, and 40, respectively. It can be seen that the population number had a greater impact on the optimization results. The Pareto frontier gradually dispersed with an increasing population number, but the thermal efficiency converged to about 14%, and the SIC value gradually increased. Therefore, the population size was set to 30. The Pareto frontier with different iterations is shown in Figure 8, and the maximum iterations were set to 30, 300, 500, and 1000, respectively. When the maximum number of iterations was 30, it had not converged enough to form a Pareto frontier, because the number of iterations was too small and the position and velocity of the particles had not been updated to the optimal position. The increase in the number of iterations will lead to an increase in the running time of the program, and does not change the shape of the Pareto frontier, so the maximum number of iterations was set to 300. The Pareto frontier for different archive sizes are shown in Figure 9. The archive sizes were set to 20, 200, 300, and 500, respectively. The archive size was used to save the best particle situation, similar to the maximum number of iterations, and the shape of the Pareto frontier was basically unchanged after exceeding 200, and the archive size was set to 200. Therefore, the specific parameter settings are shown in Table 3.

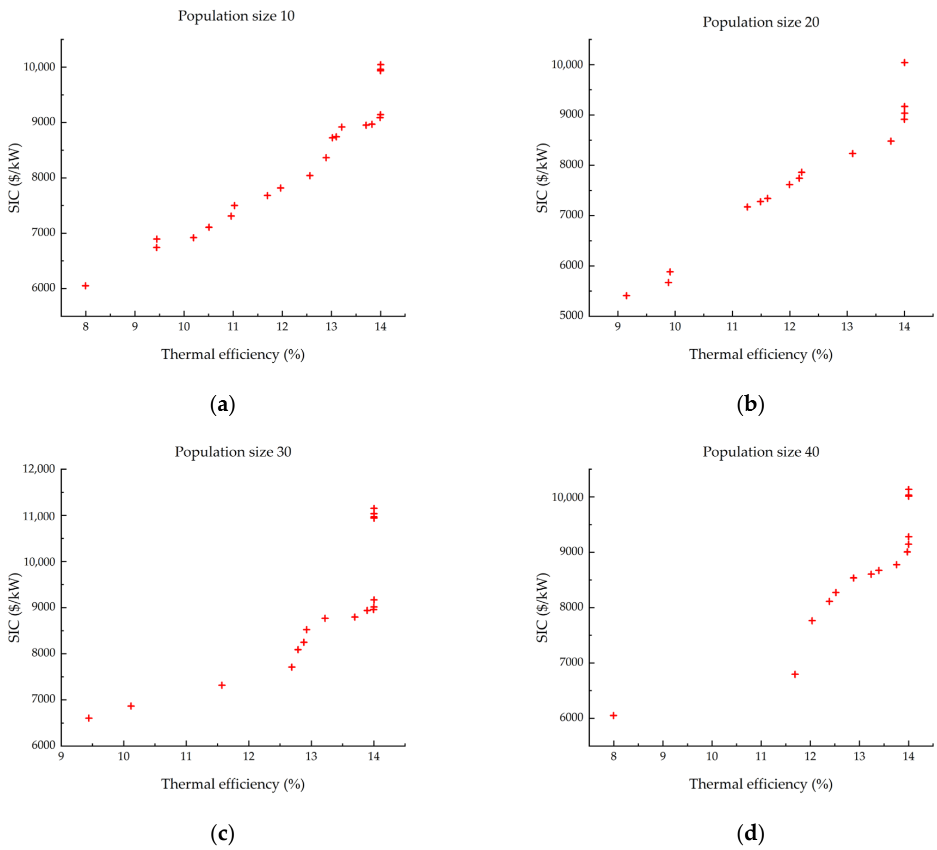

Figure 7. The effect of population size on the optimization results: (**a**–**d**) Population sizes were 10, 20, 30, and 40, respectively.

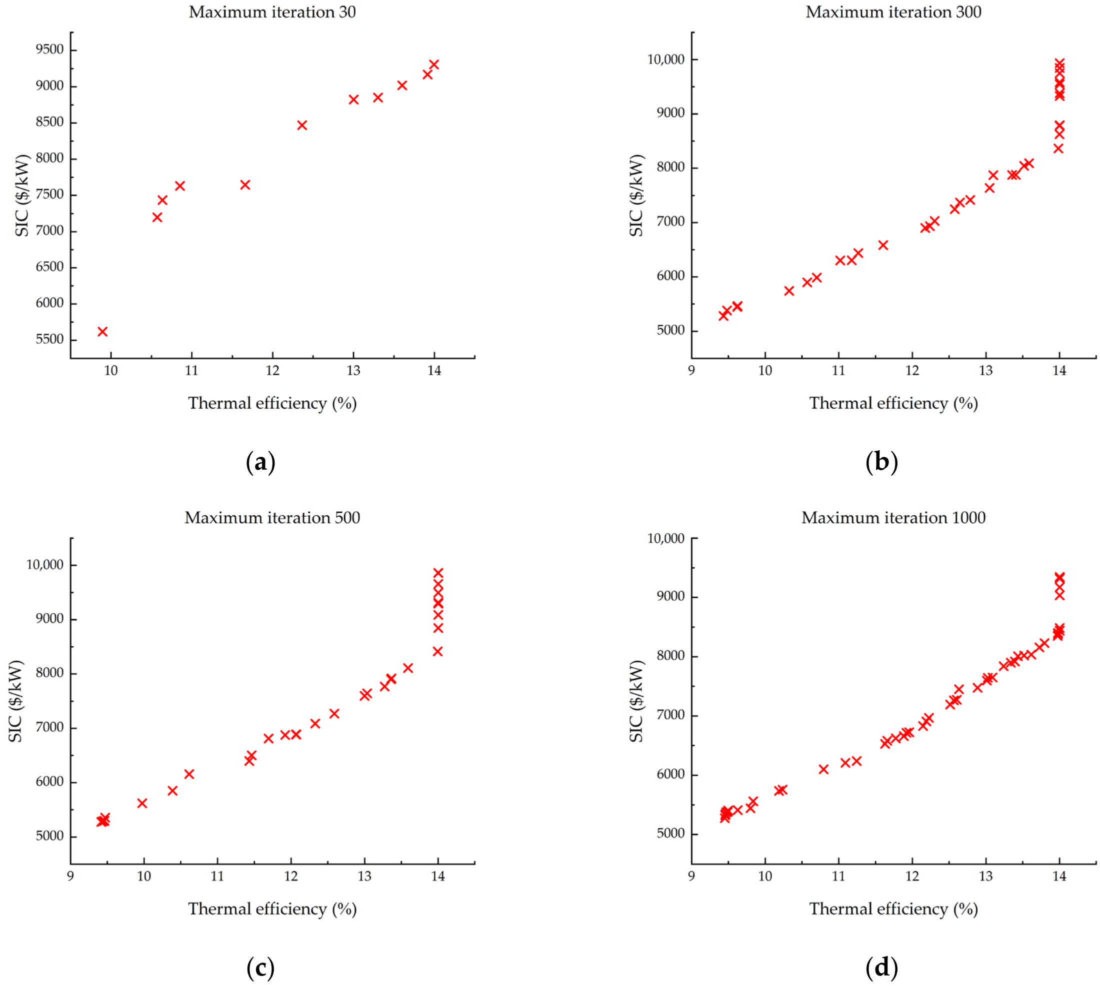

Figure 8. The effect of the maximum number of iterations on the optimization results: (**a**–**d**) Maximum iteration was 30, 300, 500 and 1000, respectively.

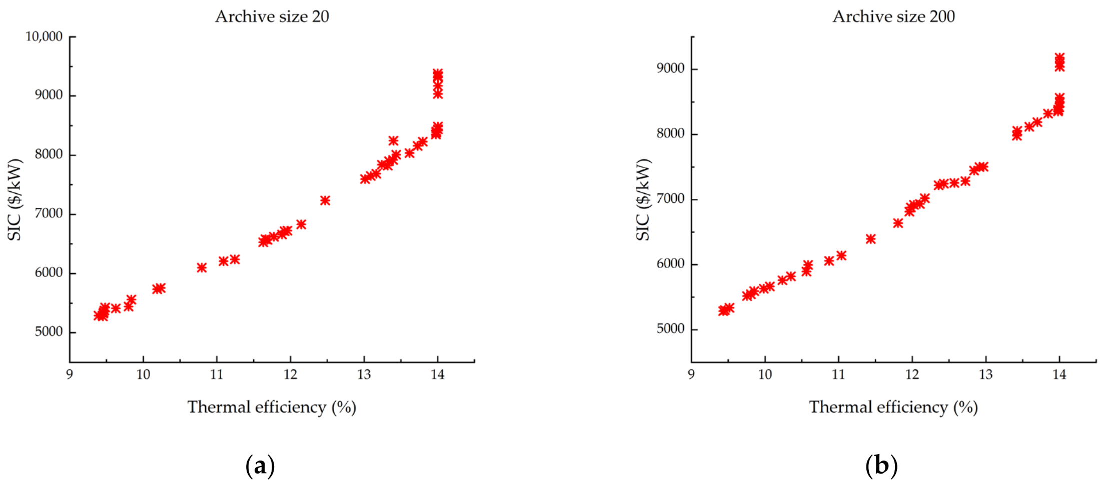

Figure 9. *Cont.*

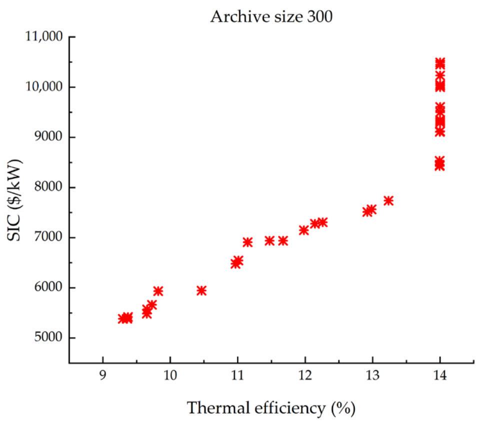

(**c**)

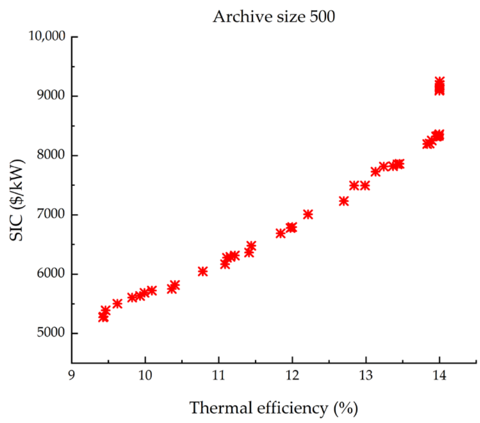

(**d**)

Figure 9. The effect of the archive size on the optimization results: (**a**–**d**) Archive sizes were 20, 200, 300, and 500, respectively.

Table 3. Optimized model parameter settings.

Parameter	Value
Population numbers	30
Maximum number of iterations	300
Archive size	200
Mutation probability	0.1
Inertia weight factor	0.9
Learning Factor	1.7/1.8

2.5. Multi-Objective Optimization Decision Method

Unlike single-objective optimization problems, the solution set of multi-objective optimization problems often does not have an optimal solution, and the solution set has a Pareto frontier. The multi-objective optimization objectives often interact with each other or even contradict each other, and the decision-making process of selecting an optimal solution from the Pareto frontier according to the actual situation is very complicated. The results studied by Basílio [47] showed, in the multi-objective decision approach, that the analytic hierarchy process(AHP) and TOPSIS approaches had the most publications in the four decades (1977–2022) and were also the most commonly employed methods in solving multi-objective related issues. Computer science stands out among others because 47% of the methods address issues related to these areas, with the TOPSIS method being used the most. Engineering follows, with 35% of the methods, with the AHP method being the second most commonly used method. Therefore, TOPSIS was used to make a decision on the multi-objective optimization.

The basic principle of TOPSIS is based on the concept that the chosen alternative should have the shortest geometric distance from the positive ideal solution and the longest geometric distance from the negative ideal solution. If the evaluation object is closest to the positive ideal solution and farthest away from the negative ideal solution at the same time, it is the best, otherwise it is not optimal. Due to the different dimensions, it is often necessary to perform dimensionless processing on the optimization parameters. In this paper, the maximum and minimum method was used to perform the dimensionless processing of the decision-making objective, and the TOPSIS method was used to perform the decision processing on the Pareto solution set.

The distance between the target alternative and the positive ideal solution and the distance between the target alternative and the negative ideal solution were calculated as shown in Equations (23) and (24), respectively.

$$d_{i+} = \sqrt{\sum_{j=1}^{n}\left(F_{ij} - F_j^{ideal}\right)^2} \tag{23}$$

$$d_{i-} = \sqrt{\sum_{j=1}^{n}\left(F_{ij} - F_j^{non-ideal}\right)^2} \tag{24}$$

Equation (25) calculates the closeness of the optimization result to the positive ideal solution. The higher the value of C_i, the closer it is to the positive ideal solution.

$$C_i = \frac{d_{i-}}{d_{i+} + d_{i-}} \tag{25}$$

As shown in Figure 10, it describes how to find the optimal solution in a Pareto frontier. Since the goal in this paper was to have a greater efficiency and a smaller SIC value, the point in the lower right corner was the positive ideal solution and the upper left corner was the negative ideal solution. The closeness of each Pareto solution to the ideal solution was calculated through the equations, and the closest one was the optimal solution determined by the decision.

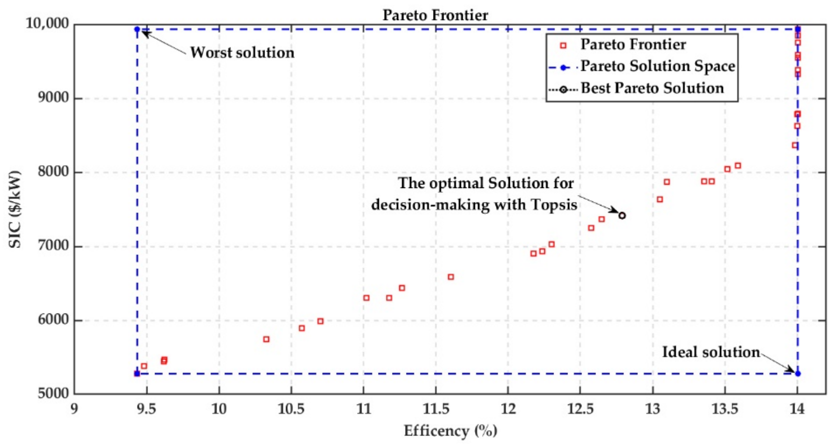

Figure 10. The selection of the optimal solutions in the Pareto frontier.

3. Results and Discussion

3.1. Single-Operating Condition Optimization Results Analysis

Figure 11 shows the effect of the ORC operating parameters on the thermal efficiency and SIC with the engine speed of 2250 rpm at full load. From Figure 11a, it can be seen that the thermal efficiency of ORC and SIC increased with the increase on the evaporating pressure. This is mainly because the enthalpy of the inlet of the expander increases with the increase in the evaporating pressure, which leads to an increase in the work capacity of the expander, so both the heat transfer area and the net output power increase, making the thermal efficiency and SIC value increase. In Figure 11b, the net ORC output power decreased as the condensing pressure increased, resulting in a continuous decrease in the thermal efficiency while the SIC value increased. In Figure 11c, the degree of superheating had little effect on the thermal efficiency of the cycle, but has a greater impact on the SIC value. The reason for the analysis is that the degree of superheating is a physical quantity used to ensure that the working fluid is in a superheated state at the inlet of the expander. In Figure 11d, as the degree of subcooling increased, the thermal efficiency decreased and the SIC value increased. This is because the temperature of the working fluid at the inlet of the pump decreased, and when the evaporating and condensing pressures remained unchanged, the power consumed by the pump during the isentropic process increased, resulting in a decrease in the net output power and thermal efficiency, and the SIC value increased.

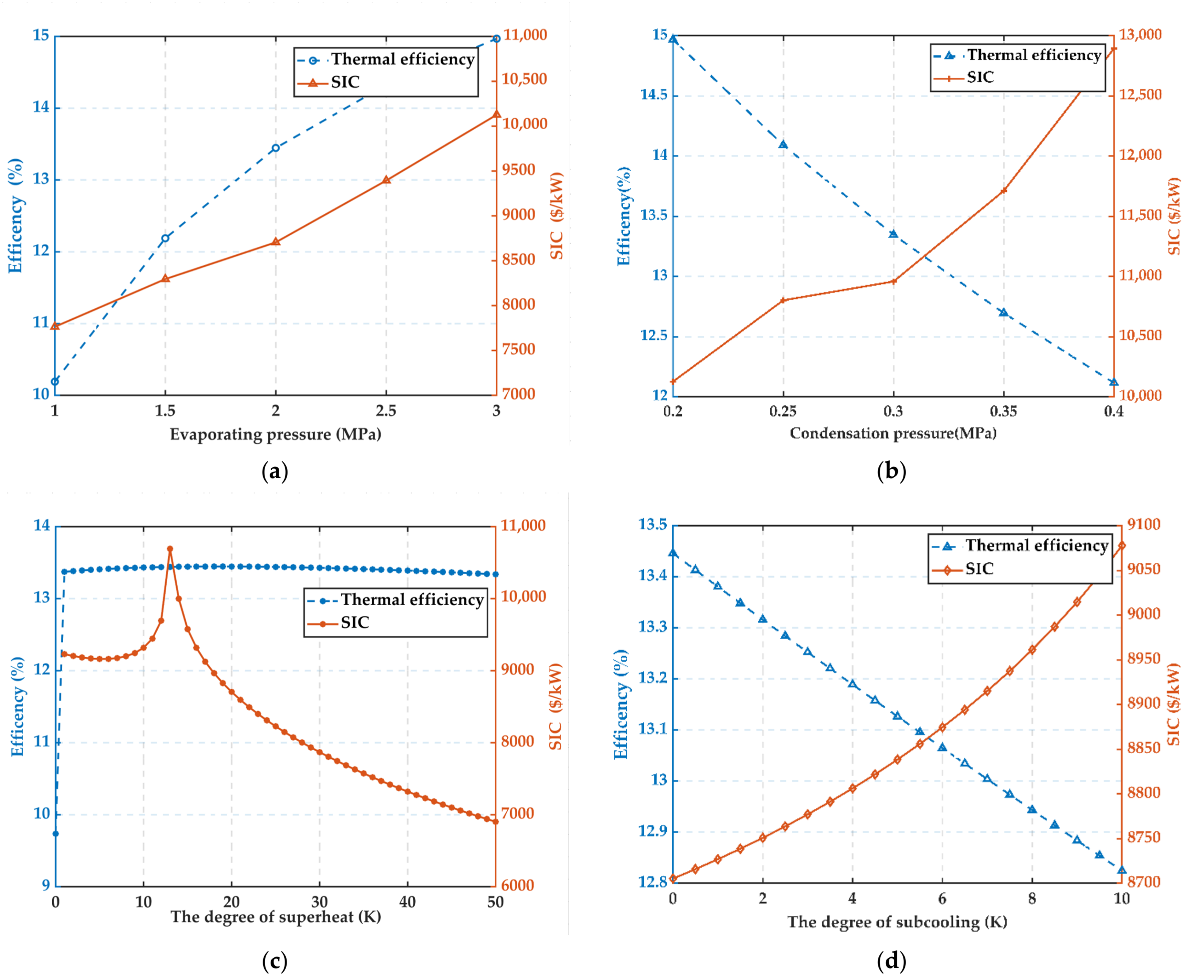

Figure 11. The effect of the ORC operating parameters on the two objectives with the engine speed of 2250 rpm at the full load: (**a**) evaporation pressure; (**b**) condensation pressure; (**c**) the degree of superheating; (**d**) the degree of subcooling.

3.2. Multi-Operating Conditions Optimization Results Analysis

In this paper, PSO was used to optimize the thermal efficiency and economic index SIC of the ORC system as the objective function under the operating conditions of the diesel engine from 850 rpm to 4500 rpm with 25%, 50%, 75% and 100% load, respectively. The optimization calculation results are presented in Figure 12. Figure 12a shows the variation in the optimal values of the evaporating and condensation pressure of the working fluid with the diesel engine operating conditions. The optimized evaporating pressure decreased with the increase in the torque and engine speed, the operating conditions had little effect on the condensing pressure and its value basically kept the minimum value of about 0.1 MPa within the given range, while the evaporating pressure ranged from 1.4 MPa to 3 MPa. Higher evaporating pressure will increase the power consumed by the pump, so in order to ensure the optimal SIC value target, when the output net power does not change much, the cost can be reduced by decreasing the pump power consumption. Figure 12b shows the variation in the degree of superheating and subcooling with engine speed and torque for the optimized ORC system. The optimized superheat range was between 1 and 10 K and the subcooling range was between 0 and 4.5 K under variable engine operating conditions. The graph shows that in most cases, the degree of superheating was the maximum value in a given range and the subcooling was the minimum value. This is because a higher superheat makes the working fluid at the evaporator outlet have a larger enthalpy, which makes the expander work harder, while a smaller subcooling makes the pump consume less power. Figure 12c shows the mass flow rate of the working fluid increased with the increase in the torque and engine speed. The exhaust mass flow rate was small under low and medium engine speed and torque, and obtained between 0 and 0.05 kg/s; when the engine speed was at 4500 rpm, the mass flow rate of the working fluid could reach a maximum of 0.23 kg/s. In Figure 12d, the variation law of the net output power of the ORC system was similar to the brake power of the diesel engine, and both increased with the increase in the engine torque and speed. This is mainly because the exhaust temperature and mass flow rate increase with the increase in the diesel engine speed and torque, so the exhaust energy that can be utilized by the ORC system also increases and leads to the net output power increases accordingly. When the engine speed was 4500 rpm with a full load at 216.7 N·m, the net output power of the ORC system reached the maximum power of 8.31 kW.

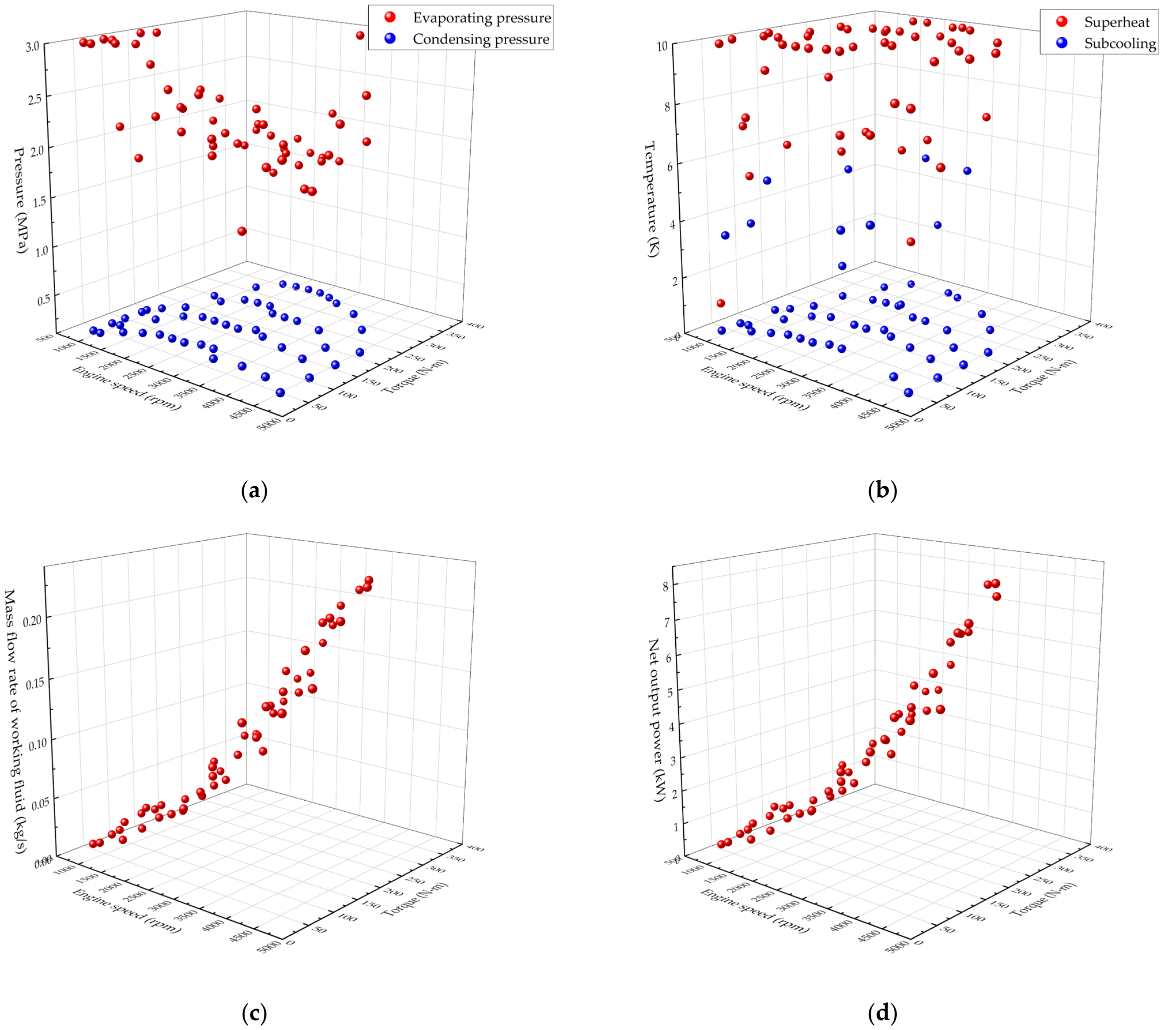

Figure 12. The effect of the multi-operating conditions optimization results: (**a**) evaporating and condensing pressure; (**b**) the degree of superheat and subcooling; (**c**) mass flow rate of working fluid; (**d**) ORC net output power.

In Figure 13a, the thermal efficiency of the ORC system increased with the increase in the engine speed and torque, the optimized range was from 10.72% to 12.76% and could reach the maximum efficiency at full load and an engine speed of 3500 rpm. In Figure 13b, the SIC value decreased with the increase in speed and torque. This is because the net output power increased with an increase in the speed and torque, and from Equation (20), the SIC value decreased.

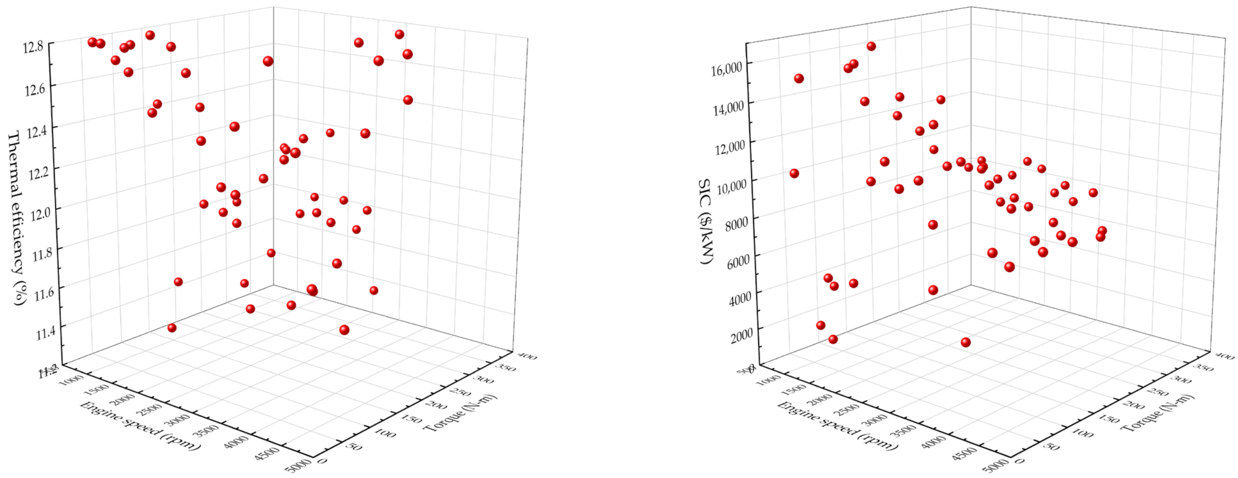

(**a**) (**b**)

Figure 13. The optimization results of the two objectives: (**a**) thermal efficiency; (**b**) SIC.

3.3. Thermo-Economic Optimization Results Analysis

In the process of TOPSIS multi-objective decision-making, when the optimal situation is selected under a single operating condition, it is actually a balanced state, and one of the objectives is often not the optimal situation. In Figure 10, the thermal efficiency of the optimal solution did not reach the maximum value, which is the ideal solution in the figure, and the SIC was not taken to the minimum value, which is the worst solution, that can be seen as a loss of part of the thermal efficiency to improve the economic efficiency in this case. Taking the data shown in Figure 10, considering the maximum thermal efficiency under this operating condition and the maximum SIC as the initial situation, the optimal solution obtained by the decision can be regarded as reducing the thermal efficiency by 7.93%, but increasing the thermal efficiency by 16.72% in terms of economic benefits.

Figure 14 shows the ORC thermal efficiency loss rate and economic efficiency improvement rate of the optimization decision results under all of the operating conditions. Figure 14a represents the loss rate of thermal efficiency relative to the optimal solution under this operating condition, and Figure 14b indicates the economic benefit relative to the worst solution at this operating condition. The improvement rate in the economic benefits gradually decreased with the increase in the engine speed and torque. In the medium and low speed and load ranges, reducing the thermal efficiency can appropriately improve the economic benefits. When the engine was 1250 rpm and the load rate was 50%, the largest thermal efficiency loss rate was 0.12, and the corresponding economic improvement rate also reached the maximum value of 0.83; while at a 4000 rpm full load, the economic benefit improvement rate reached the minimum value of 0.03, which indicates that the economic and thermal benefits of the ORC system reached a relative balance when the system was under heavy load conditions, and it was difficult to improve the economic benefit by changing the thermal efficiency. Therefore, in the practical application of the ORC system, the economic benefit can be improved by reducing a part of the thermal efficiency at low and medium engine speeds and torques, while the thermal efficiency target is dominant at high speeds and high torques.

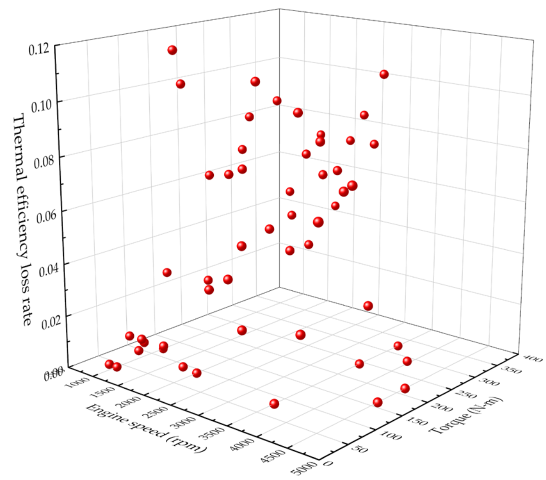

(**a**)

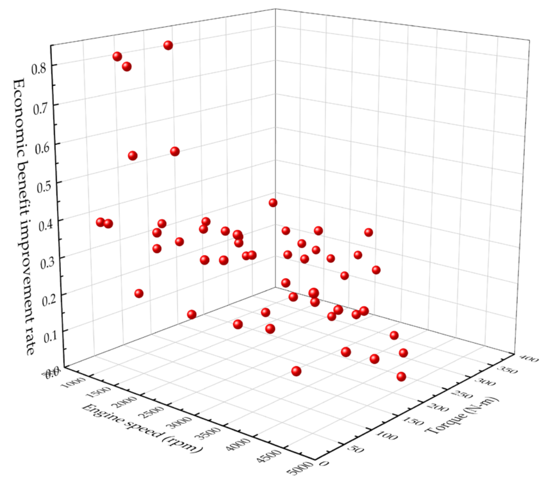

(**b**)

Figure 14. The optimization results of the two objectives: (**a**) thermal efficiency loss rate; (**b**) economic benefit improvement rate.

Figure 15 represents the variation in the BSFC optimization. The BSFC had a similar variation pattern before and after the addition of the ORC system, but the value after the addition of the ORC system decreased significantly compared to that before the optimization, with a maximum decrease of 8.3%. This is because the BSFC of the engine–ORC combined system is not only affected by parameters such as fuel consumption and brake power, but also by the net output power of the ORC system. When the engine speed was 1750 rpm and the torque was 354.90 N-m, the BSFC value of the combined system was the lowest, which was 238.9 g/(kW·h)$^{-1}$.

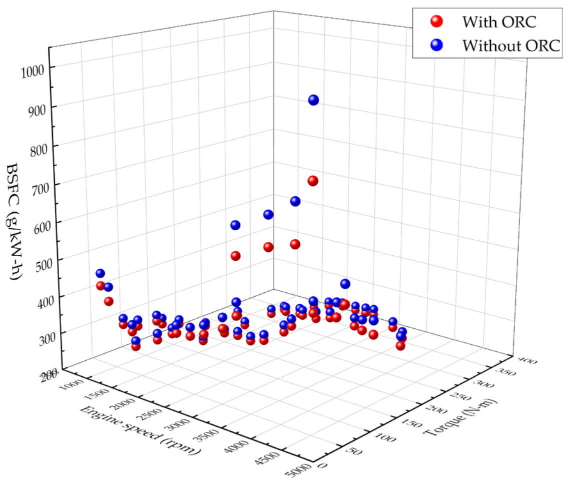

Figure 15. The comparison of BSFC with ORC.

3.4. Bench Test and Model Validation

The mass flow rate of the working fluid, the net output power, and thermal efficiency of the ORC system under the full load condition of the engine speed from 850 rpm to 4500 rpm were measured through the test rig. Taking the inlet temperature, mass flow rate, and pressure of the exhaust and working fluid as input parameters of the PSO program, the degree of superheating was set to 10, the degree of subcooling was set to 0, the mass flow rate of the coolant water was 0.15 kg/s, and the net output power and thermal efficiency of the ORC system were obtained. The comparison of the test rig, PSO numerical calculation, and BPNN fitting prediction result data are shown in Figure 16. It can be seen from the figure that the PSO numerical calculation program and the BPNN fitting results were basically consistent with the test rig results. Except at 3500 rpm, the relative errors of the PSO and BPNN results and the test rig were not more than 5%.

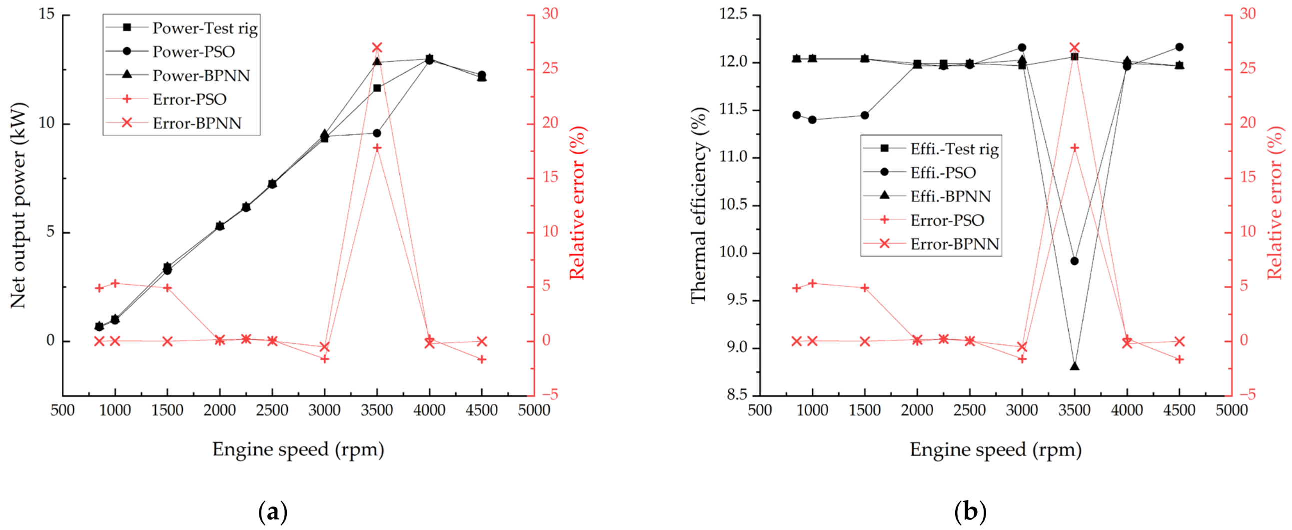

Figure 16. The comparison of the performance prediction models for the 10 test conditions with full load at different speeds: (**a**) net output power; (**b**) thermal efficiency.

4. Conclusions

1. The engine–ORC combined system can recover the exhaust energy of a tractor diesel engine. When the engine speed was 3500 rpm and full load torque was 323.8 N-m, the ORC thermal efficiency reached a maximum of 12.76% and the corresponding SIC value was 8539.66 $/kW. When the engine speed was 4500 rpm and the full load torque was 216.7 N m, the net output power of the ORC system was up to 8.31 kW. When the engine speed was 1750 rpm, the full load torque was 354.90 N·m, it had the minimum BSFC value of 238.9 $g/(kW \cdot h)^{-1}$ with the addition ORC system, and compared to the engine without the ORC system, the BSFC improvement was 8.3%.
2. The analysis of a single-case operating condition shows that with the increase in the evaporating pressure, the ORC thermal efficiency and SIC value will continue to increase, and when the condensation pressure is increased, the ORC thermal efficiency will decrease and the SIC value increase; increasing the ORC working fluid superheating had little effect on the thermal efficiency. The SIC value first increased and then decreased while the continuous increase of the degree of subcooling led to a decrease in the thermal efficiency and an increase in the SIC value.
3. The multi-objective optimization results showed that the optimal value of the evaporation pressure varied from 1.4 MPa to 3 MPa, the condensing pressure was less affected by the change in the working conditions, and was basically maintained at about 0.1 MPa. The optimized degree of superheating and subcooling were in the ranges of 1–10 K and 0–4.5 K, respectively. The mass flow of the working fluid was mainly affected by the operating conditions of the diesel engine. The optimized ratio of the mass flow rate of the working fluid to the exhaust was between 1.2 and 1.5. Under the conditions of low and medium speed and torque, the exhaust mass flow was small and the temperature was relatively low, and the working fluid mass flow varied between 0 and 0.05 kg/s, which increased with the increase in the engine speed and torque, and reached a maximum value of 0.23 kg/s at 4500 rpm under full load conditions. In most operating conditions, the ORC thermal efficiency remained around 12%. When the engine ran in the medium and high load region, the ORC system showed better thermal economy, and the maximum value was 12.76% under a full load at 3500 rpm.

4. For the ORC, the improvement in the thermodynamic performance will inevitably lead to a sacrifice in economic performance, so economic benefits can be improved by reducing a part of the thermal efficiency. The analysis of the Pareto frontier under each operating condition showed that the loss rate of thermal efficiency was between 0 and 0.12, and the improvement rate in the economic benefits was 0 to 0.83. When the loss rate of thermal efficiency was the largest, the corresponding economic improvement rate could also reach the maximum value. At low and medium speeds, there was an obvious conflict between the thermal efficiency and economic benefits, and the economic benefits could be improved by appropriately reducing the thermal efficiency in the process of practical application, while at high speeds, the economic benefits and thermal efficiency reached a balance and showed a better thermal economic performance.
5. Through the test rig, the performance parameters of the engine at 850–4500 rpm including 10 different speeds and loads, a total of 210 operating conditions were measured. The net output power and thermal efficiency of the ORC system with all of the operating conditions were obtained by adjusting the mass flow rate and pressure of the working fluid to verify the validity of the developed thermodynamic model. Comparing the test rig collected data with the PSO model optimization and the BPNN prediction results, it was found that, except at 3500 rpm, the maximum relative errors of the thermal efficiency and net power output were 5.3% and 5.585%, respectively, indicating that the PSO optimization model established in this paper has certain validity and usability.

Author Contributions: Conceptualization, W.P. and M.T.; Methodology, W.P and M.T.; Software, W.P. and G.Z.; Validation, W.P., J.L., and L.Z.; Formal analysis, W.P., J.L., and M.T.; Investigation, W.P.; Resources, M.T.; Data curation, G.Z. and M.T.; Writing—original draft preparation, W.P. and J.L.; Writing—review and editing, W.P. and M.T.; Visualization, W.P., G.Z., and M.T.; Supervision, M.T.; Project administration, W.P. and M.T.; Funding acquisition, M.T. All authors have read and agreed to the published version of the manuscript.

Funding: This research was funded by the Fundamental Research Funds for the Central Universities, grant number 2662020GXPY016, the China Agriculture Research System of MOF and MARA, grant number CARS-24-D-02, and the National Natural Science Foundation of China, grant number 51605182.

Institutional Review Board Statement: Not applicable.

Informed Consent Statement: Not applicable.

Data Availability Statement: Not applicable.

Conflicts of Interest: The authors declare no conflict of interest.

Abbreviations

ANFIS	Adaptive neuro-fuzzy inference system
BPNN	Back propagation neural network
BSFC	Brake specific fuel consumption
DRL	Deep reinforcement learning
EKF	Extended Kalman filter
EMS	Energy management system
GA	Genetic algorithm
GD-LSE	Gradient-descent least-square estimate
LMTD	Log mean temperature difference
MOGA	Multi-objective genetic algorithm
NETL	National energy technology laboratory
NMPC	Nonlinear model predictive controller
ORC	Organic Rankine cycle
PSO	Particle swarm optimization

SIC	Specific investment cost
SVR	Support vector regression
TC	Total cost
TOPSIS	Technique for order of preference by similarity to ideal solution
WHR	Waste heat recovery
Nomenclature	
η	Efficiency
a_0	Scaling factor
A	Heat transfer area
C	Cost
D	Hydraulic diameter of the flow channel
F	Forced convective heat transfer enhancement factor, function value
h	Heat transfer coefficient
i	Specific enthalpy
k	Thermal conductivity
$\dot{m}$	Mass flow rate
Nu	Nusselt number
P	Pressure
Pr	Prandtl number
$\dot{Q}$	Heat absorb by the refrigerant
Re	Reynolds number
S	Forced convective heat transfer suppression factor
T	Temperature
U	Total heat transfer coefficient
$\dot{W}$	Output power by expander
Subscripts	
1–16	State point
cp	Component cost
e	Exhaust
ev	Two-phase
exp	Expander
exp,iso	Isentropic efficiency of the expander
hx	Heat exchanger
lab	Labor cost
$motor$	Electric motor
$pool$	Pooling boiling transfer coefficient
$pump$	ORC pump
$pump,iso$	Isentropic efficiency of the pump
r	Refrigerant
wf	Working fluid

References

1. National Bureau of Statistics of China. Available online: https://www.stats.gov.cn/ (accessed on 19 July 2022).
2. Lang, J.L.; Tang, J.J.; Zhou, Y.; Li, K.H.; Chen, D.S.; Huang, Q.; Xing, X.F.; Zhang, Y.Y.; Cheng, S.Y. A high temporal-spatial resolution air pollutant emission inventory for agricultural machinery in China. *J. Clean. Prod.* **2018**, *183*, 1110–1121. [CrossRef]
3. Zhang, Y.H.; Lou, D.M.; Tan, P.Q.; Hu, Z.Y.; Fang, L. Emission characteristic of non-road mobile machinery using a catalysed diesel particle filter with different catalyst loadings under actual operating conditions. *J. Clean. Prod.* **2021**, *327*, 1–12. [CrossRef]
4. Bacenetti, J.; Lovarelli, D.; Facchinetti, D.; Pessina, D. An environment comparison of techniques to reduce pollutants emissions related to agricultural tractors. *Biosyst. Eng.* **2018**, *171*, 30–40. [CrossRef]
5. Janulevičius, A.; Šarauskis, E.; Čiplienė, A.; Juostas, A. Estimation of farm tractor performance as a function of time efficiency during ploughing in fields of different sizes. *Biosyst. Eng.* **2019**, *179*, 80–93. [CrossRef]
6. Omar, A.; Saghafifar, M.; Mohammadi, K.; Alashkar, A.; Gadalla, M. A review of unconventional bottoming cycles for waste heat recovery: Part II-Applications. *Energy Conv. Manag.* **2019**, *180*, 559–583. [CrossRef]
7. Punov, P.; Lacour, S.; Périlhon, C.; Podevin, P.; Descombes, G.; Evtimov, T. Numerical study of the waste heat recovery potential of the exhaust gases from a tractor engine. *Proc. Inst. Mech. Eng. Part D J. Automob. Eng.* **2015**, *230*, 37–48. [CrossRef]

8. Hu, S.; Yang, Z.; Li, J.; Duan, Y. A review of multi-objective optimization in organic Rankine cycle (ORC) system design. *Energies* **2021**, *14*, 6492. [CrossRef]
9. Lion, S.; Michos, C.N.; Vlaskos, I.; Rouaud, C.; Taccani, R. A review of waste heat recovery and organic Rankine cycles (ORC) in on-off highway vehicle heavy duty diesel engine applications. *Renew. Sust. Energ. Rev.* **2017**, *79*, 691–708. [CrossRef]
10. Kalinichenko, A.; Havrysh, V.; Hruban, V. Heat recovery systems for agricultural vehicles: Utilization ways and their efficiency. *Agriculture* **2018**, *8*, 199. [CrossRef]
11. Punov, P.; Lacourm, S.; Perilhon, C.; Podevin, P. Possibilities of waste heat recovery on tractor engines. In Proceedings of the International Scientific Conference on Aeronautics, Automotive and Railway Engineering and Technologies, Sofia, Bulgaria, 16–18 October 2013.
12. Vaupel, Y.; Schulze, J.C.; Mhamdi, A.; Mitsos, A. Nonlinear model predictive control of organic Rankine cycles for automotive waste heat recovery: Is it worth the effort? *J. Process Control* **2021**, *99*, 19–27. [CrossRef]
13. Vaupel, Y.; Huster, W.R.; Mhamdi, A.; Mitsos, A. Optimal operating policies for organic Rankine cycles for waste heat recovery under transient conditions. *Energy* **2021**, *224*, 120126. [CrossRef]
14. Mohammadkhani, F.; Yari, M. A 0D model for diesel engine simulation and employing a transcritical dual loop Organic Rankine Cycle (ORC) for waste heat recovery from its exhaust and coolant: Thermodynamic and economic analysis. *Appl. Therm. Eng.* **2019**, *150*, 329–347. [CrossRef]
15. Wang, Q.; Wu, W.; Li, D.; Wang, J.; He, Z. Thermodynamic analysis and optimization of four organic flash cycle systems for waste heat recovery. *Energy Conv. Manag.* **2020**, *221*, 113171. [CrossRef]
16. Zhang, W.; Yang, F.; Zhang, H.; Ping, X.; Yan, D.; Wang, C. Application of two-phase pulsating flow in organic Rankine cycle system for diesel engine waste heat recovery. *Energy* **2022**, *243*, 122776. [CrossRef]
17. Teng, S.; Feng, Y.-Q.; Hung, T.-C.; Xi, H. Multi-objective optimization and fluid selection of different cogeneration of heat and power systems based on organic Rankine cycle. *Energies* **2021**, *14*, 4967. [CrossRef]
18. Zhou, Y.; Li, S.; Sun, L.; Zhao, S.; Talesh, S.S. Optimization and thermodynamic performance analysis of a power generation system based on geothermal flash and dual-pressure evaporation organic Rankine cycles using zeotropic mixtures. *Energy* **2020**, *194*, 116785. [CrossRef]
19. Welcome to CoolProp. Available online: https://www.coolprop.org/ (accessed on 19 July 2022).
20. National Institute of Standards and Technology; US Department of Commerce. NIST Reference Fluid Thermodynamic and Transport Properties Database (REFPROP). Available online: https://www.nist.gov/srd/refprop (accessed on 19 July 2022).
21. Redjeb, Y.; Kaabeche-Djerafi, K.; Stoppato, A.; Benato, A. The IRC-PD Tool: A Code to Design Steam and Organic Waste Heat Recovery Units. *Energies* **2021**, *14*, 5611. [CrossRef]
22. Ping, X.; Yang, F.; Zhang, H.; Zhang, W.; Zhang, J.; Song, G.; Wang, C.; Yao, B.; Wu, Y. Prediction and optimization of power output of single screw expander in organic Rankine cycle (ORC) for diesel engine waste heat recovery. *Appl. Therm. Eng.* **2021**, *182*, 116048. [CrossRef]
23. Zhang, W.; Yang, F.; Zhang, H.; Ping, X.; Yan, D. Numerical analysis and optimization design of fin-and-tube evaporator in organic Rankine cycle system for diesel engine waste heat recovery. *Int. J. Heat Mass Transf.* **2021**, *175*, 121376. [CrossRef]
24. Ping, X.; Yang, F.; Zhang, H.; Zhang, J.; Zhang, W.; Song, G. Introducing machine learning and hybrid algorithm for prediction and optimization of multistage centrifugal pump in an ORC system. *Energy* **2021**, *222*, 120007. [CrossRef]
25. Duarte-Forero, J.; Obregón-Quiñones, L.; Valencia-Ochoa, G. Comparative analysis of intelligence optimization algorithms in the thermo-economic performance of an energy recovery system based on organic rankine cycle. *J. Energy Resour. Technol-Trans. ASME* **2021**, *143*, 1–18. [CrossRef]
26. Liu, H.; Zhang, H.; Yang, F.; Hou, X.; Yu, F.; Song, S. Multi-objective optimization of fin-and-tube evaporator for a diesel engine-organic Rankine cycle (ORC) combined system using particle swarm optimization algorithm. *Energy Conv. Manag.* **2017**, *151*, 147–157. [CrossRef]
27. Ren, L.; Liu, J.; Wang, H. Thermodynamic Optimization of a Waste Heat Power System under Economic Constraint. *Energies* **2020**, *13*, 3388. [CrossRef]
28. Feng, Y.-q.; Liu, Y.-Z.; Wang, X.; He, Z.-X.; Hung, T.-C.; Wang, Q.; Xi, H. Performance prediction and optimization of an organic Rankine cycle (ORC) for waste heat recovery using back propagation neural network. *Energy Conv. Manag.* **2020**, *226*, 113552. [CrossRef]
29. Wang, W.; Deng, S.; Zhao, D.; Zhao, L.; Lin, S.; Chen, M. Application of machine learning into organic Rankine cycle for prediction and optimization of thermal and exergy efficiency. *Energy Conv. Manag.* **2020**, *210*, 112700. [CrossRef]
30. Han, Z.; Jia, X.; Li, P. Preliminary design of radial inflow turbine and working fluid selection based on particle swarm optimization. *Energy Conv. Manag.* **2019**, *199*, 111933. [CrossRef]
31. Zhao, M.; Canova, M.; Tian, H.; Shu, G. Design space exploration for waste heat recovery system in automotive application under driving cycle. *Energy* **2019**, *176*, 980–990. [CrossRef]
32. Chowdhury, J.; Nguyen, B.; Thornhill, D.; Hu, Y.; Soulatiantork, P.; Balta-Ozkan, N.; Varga, L. Fuzzy nonlinear dynamic evaporator model in supercritical organic rankine cycle waste heat recovery systems. *Energies* **2018**, *11*, 901. [CrossRef]
33. Enayatollahi, H.; Sapin, P.; Unamba, C.K.; Fussey, P.; Markides, C.N.; Nguyen, B.K. A Control-oriented ANFIS model of evaporator in a 1-kWe organic Rankine cycle prototypr. *Electronics* **2021**, *10*, 1535. [CrossRef]

34. Wang, H.; Zhang, H.; Yang, F.; Song, S.; Chang, Y.; Bei, C.; Yang, K. Parametric optimization of regenerative organic rankine cycle system for diesel engine based on particle swarm optimization. *Energies* **2015**, *8*, 9751–9776. [CrossRef]
35. Fergani, Z.; Morosuk, T.; Touil, D. Exergy-based multi-objective optimization of an organic rankine cycle with a zeotropic mixture. *Entropy* **2021**, *23*, 954. [CrossRef]
36. Luo, H.; Zhou, P.; Shu, L.; Mou, J.; Zheng, H.; Jiang, C.; Wang, Y. Energy performance curves prediction of centrifugal pumps based on constrained PSO-SVR model. *Energies* **2022**, *15*, 3309. [CrossRef]
37. Chowdhury, J.; Nguyen, B.; Thornhill, D. Modelling of evaporator in waste heat recovery system using finite volume method and fuzzy technique. *Energies* **2015**, *8*, 14078–14097. [CrossRef]
38. Wang, X.; Wang, R.; Shu, G.; Tian, H.; Zhang, X. Energy management strategy for hybrid electric vehicle integrated with waste heat recovery system based on deep reinforcement learning. *Sci. China Tech. Sci.* **2021**, *65*, 713–725. [CrossRef]
39. Rathod, D.; Xu, B.; Filipi, Z.; Hoffman, M. An experimentally validated, energy focused, optimal control strategy for an organic Rankine cycle waste heat recovery system. *Appl. Energy* **2019**, *256*, 113991. [CrossRef]
40. Hoffman, M.; Filipi, Z.; Onori, S.; Rathod, D.; Yebi, A.; Xu, B. Experimental validation of nonlinear model predictive control for a heavy-duty diesel engine waste heat recovery system. *J. Dyn. Syst. Meas. Control* **2020**, *142*, 51001.
41. Bejan, A. *Convection Heat Transfer*, 4th ed.; John Wiley & Sons: New Jersey, NJ, USA, 2013; pp. 106–107.
42. Liu, Z.; Winterton, R.H.S. A general correlation for saturated and subcooled flow boiling in tubes and annuli, based on a nucleate pooling boiling equation. *Int. J. Heat Mass Transfer.* **1991**, *34*, 2759–2766. [CrossRef]
43. Lecompte, S.; Lemmens, S.; Huisseune, H.; Van den Broek, M.; De Paepe, M. Multi-objective thermo-economic optimization strategy for orcs applied to subcritical and transcritical cycles for waste heat recovery. *Energies* **2015**, *8*, 2714–2741. [CrossRef]
44. Quoilin, S.; Declaye, S.; Tchanche, B.; Lemort, V. Thermo-economic optimization of waste heat recovery organic Rankine cycles. *Appl. Therm. Eng.* **2011**, *31*, 2885–2893. [CrossRef]
45. Pantaleo, A.; Simpson, M.; Rotolo, G.; Distaso, E.; Oyewunmi, O.; Sapin, P.; De Palma, P.; Markides, C. Thermoeconomic optimisation of small-scale organic Rankine cycle systems based on screw vs. piston expander maps in waste heat recovery applications. *Energy Conv. Manag.* **2019**, *200*, 112053. [CrossRef]
46. Astolfi, M. Techno-economic optimization of low temperature CSP systems based on ORC with screw expanders. *Energy Proc.* **2015**, *69*, 1100–1112. [CrossRef]
47. Basílio, M.; Pereira, V.; Costa, H.; Santos, M.; Ghosh, A. A systematic review of the applications of multi-criteria decision aid methods (1977–2022). *Electronics* **2022**, *11*, 1720. [CrossRef]